Journal of Materials Chemistry A

ROYAL SOCIETY OF CHEMISTRY

PAPER

View Article Online
View Journal | View Issue



Cite this: J. Mater. Chem. A, 2025, 13, 34440

# Combining low viscosity and high volumetric redox density of organic polymers for energy-efficient catholytes in redox flow batteries: a redox-active polyelectrolyte approach

Kohei Ishigami [a] and Kenichi Oyaizu *[ab]

Redox flow batteries, which combine polymeric active materials, nanoporous separators, and pH-neutral aqueous electrolytes, have the potential as low-cost, safe, grid-scale rechargeable batteries. Polymeric active materials that exhibit both high water solubility and low viscosity are limited. A rational approach is required for solubility enhancement to improve specific capacity per unit volume while minimizing viscosity increase that leads to frictional loss. In this study, redox-active polyelectrolytes were proposed as polymeric active materials for aqueous redox flow batteries. The polyelectrolyte structure consisted of a polyacrylamide main chain with a strongly hydrophilic ammonium unit substituted per hydrophobic TEMPO group. The redox-active polyelectrolyte demonstrated high solubility at concentrations greater than 2 M (54 Ah $L^{-1}$) while retaining flowability in aqueous electrolytes. The cationic ammonium groups in proximity to the nitroxide radical led to its higher oxidation potential to yield the corresponding oxoammonium polymer compared to conventional TEMPO-substituted polymers. The effective molecular design in terms of water solubility, viscosity, and electrochemical properties was indicated. Highly efficient charging and discharging at 20 Ah $L^{-1}$ (0.75 M) showed its potential as a polymeric active material comparable to the capacity of commercialized vanadium redox flow batteries.

Received 3rd May 2025
Accepted 2nd September 2025

DOI: 10.1039/d5ta03516c

rsc.li/materials-a



## Introduction

Redox flow batteries (RFBs) that use aqueous flow media have the potential to be a safe and cost-effective technology for grid-scale energy storage.[1,2] In particular, vanadium redox flow batteries (VRFBs) have the advantages of high cycle stability, low self-discharge capability, and flame resistance.[3] However, vanadium pentoxide as the predominant source of the active material in VRFBs is an expensive metal oxide, constituting 40–45% of its total production costs. The significant price volatility of vanadium has been a substantial impediment to its commercialization.[4,5] Organic active materials have been suggested as an alternative material for cost reduction and sustainability of resources.[6] TEMPO, ferrocene, viologen, and others, reported to operate stably in pH-neutral aqueous electrolytes, are promising candidates for active materials in organic RFBs.[7–9]

Organic RFBs using polymers have also attracted much attention. Polymeric active materials effectively inhibit crossover combined with inexpensive nanoporous membranes, while retaining the fast charge transport properties of high-density redox units.[10–12] While perfluorosulfonic acid-based ion exchange membranes constitute 41% of the cost of current VRFB's cell stack,[13] the cost of porous membranes made of cellulose or polypropylene is approximately 2–20% of that of the ion exchange membranes,[10,13,14] suggesting that polymeric RFBs should offer a low-cost solution for large-scale rechargeable batteries.

A primary concern in the realm of polymeric RFBs pertains to the dynamic viscosity of polymer solutions, which increases exponentially with concentration. High viscosity should be avoided as this leads to reduced mobility of the electrolyte and pressure loss in the flow pump.[15] The upper limit of realistic capacity for polymeric RFBs has been less than 10 Ah $L^{-1}$ (0.37 M).[16–20] In previous studies, polymeric active materials were obtained by the copolymerization of hydrophobic redox-active monomers and solubility-enhancing comonomers. Solubility and specific capacity per mass were incompatible in this molecular design, although it was useful for catalytic applications, such as mediators in redox targeting flow batteries.[21,22] We anticipated that the molecular design of polyelectrolytes containing ionic functional groups in the monomer units should lead to high water solubility and consequently high volumetric redox density, despite the substitution of hydrophobic redox sites, such as TEMPO. Previous reports on redox-

[a]Department of Applied Chemistry, Waseda University, 3-4-1 Okubo, Shinjuku, Tokyo 169-8555, Japan. E-mail: oyaizu@waseda.jp
[b]Research Institute of Science Engineering, Waseda University, 3-4-1 Okubo, Shinjuku, Tokyo 169-8555, Japan

active and water-soluble homopolymers remain limited to viologen-substituted polymers for analytes.[20,23]

In this study, a highly water-soluble and redox-active polyelectrolyte was designed using polyacrylamide as the hydrophilic backbone with an ammonium-substituted TEMPO group in the side chain per repeating unit. The ammonium group was selected for its convenient introduction into the TEMPO unit through the Menshutkin reaction of 4-dimethylamino TEMPO. As TEMPO is characterized as one of the most stable organic radicals persistent even in aqueous media, it is the most widely used in radical polymers which are non-conjugated polymers with stable radicals per repeating unit[8,11] being sought for various electronic applications.[24–28] This study presents the first redox-active polymer with ammonium groups bound covalently per TEMPO group, which demonstrates remarkable electrochemical properties and viscosity behaviors during its redox reaction promising for use as a catholyte in RFBs. Notably, the polyelectrolyte dissolved much more readily in an aqueous solution of 1 M NaCl than other conventional polymeric active materials. Highly efficient charge–discharge was demonstrated even under the high concentration conditions. The permeability of the polyelectrolyte through the nanoporous membrane was only one-thousandth that of the low-molecular-weight model compound, indicating its excellent potential for use as an active material in polymeric RFBs.

## Experimental section

### Materials

Bromopropylamine hydrobromide, acryloyl chloride and 4-amino-2,2,6,6-tetramethylpiperidine were purchased from Tokyo Chemical Industry Co. Formic acid, 38% formaldehyde solution, 2,2′-azobis(2-methylpropionamidine)dihydrochloride, 30% hydrogen peroxide solution, hydrochloric acid, sodium carbonate, magnesium sulfate and deionized water were purchased from FUJIFILM Wako Pure Chemical Corp. Ammonium chloride, sodium tungstate dihydrate, sodium hydroxide, sodium chloride and other dehydrated organic solvents were purchased from Kanto Chemical Co. Ethyl viologen dibromide was purchased from Sigma-Aldrich and exchanged for chloride before use. The ion exchange resin used was Amberlite® IRA410J Cl, purchased from Organo Corp. *N*,*N*,2,2,6,6-Hexamethylpiperidine[29,30] and *N*,*N*,*N*-2,2,6,6-heptamethylpiperidinyloxy-4-ammonium chloride (TMA-TEMPO)[30,31] were synthesized as previously reported.

### Measurements

NMR spectra were recorded using a JEOL-ECX500. The electron spin resonance (ESR) spectrum was obtained using a Bruker Magnettech ESR5000. A Quantum Design MPMS SQUID-VSM magnetometer was used for magnetization measurements. Mass spectra were obtained by atmospheric-pressure chemical ionization (APCI) and electrospray ionization (ESI) methods with a Bruker Compact instrument. Infrared (IR) spectra were recorded using a JASCO FT/IR-4X with KBr pellets for powdery samples. Size exclusion chromatography (SEC) was performed using a SHIMADZU LC-20AD/CTO-20A with the attached TOSOH TSKgel G3000PWXL-column and SHIMADZU RID-10A refractive index detector (0.1 M sodium nitrate aqueous solution, flow rate: 1.0 mL $min^{-1}$, calibration reference: polyethylene glycol and polyethylene oxide). Thermogravimetric analyses (TGA) were performed using a Rigaku TG8120 under a nitrogen atmosphere. To eliminate the effect of moisture absorption, the samples were held at 90 °C for 1 hour prior to the analysis and then heated at a scan rate of 5 °C $min^{-1}$. Differential scanning calorimetry (DSC) was performed using a TA Instruments Q200 at a scan rate of 20 °C $min^{-1}$ under a nitrogen atmosphere. The evolved gas was characterized using a gas chromatograph (GC-8A, SHIMADZU, MS-5A column, Ar carrier) to detect the resulting oxygen peak at a retention time of 2.2 min.

### Solubility test

Dried **P1** (139 mg) was gradually added to 500 μL of 1 M NaCl aqueous solution in a microtube. The mixture was repeatedly sonicated while immersed in a 50 °C water bath to promote dissolution. After the solids and turbidity had visually disappeared, the sample was cooled to room temperature and left undisturbed for at least 30 minutes. This process continued until the solution became highly viscous and eventually gelled. At 4 M, the sample exhibited no detectable flow upon inversion, which was regarded as the solubility limit under these conditions.

### Electrochemical characterization

A conventional potentiostat (ALS660D, BAS) was employed for electrochemical measurements. All electrodes were purchased from BAS. A conventional three-electrode system was employed using a platinum wire (0.5 mm in diameter) wound into a coil of *ca.* 4 mm in diameter as the counter electrode and an Ag/AgCl wire as the reference electrode. Ag/AgCl electrodes were calibrated to 0.196 V *vs.* SHE with a 3 M NaCl aqueous solution as the internal solution. A glassy carbon disk with a diameter of 3 mm was used as the working electrode for cyclic voltammetry and hydrodynamic voltammetry. The electrolyte for voltammetry was a 1 M NaCl solution. All measurements were performed at room temperature near 25 °C.

### Dynamic viscosity analysis

Dynamic viscosity was evaluated by means of an SV-1A tuning fork-vibration viscometer, manufactured by A&D Co. A 2 mL solution of the active material was prepared for the viscosity measurement. The dynamic viscosity was determined by measuring the viscosity coefficient with vibration at 30 Hz divided by the solvent density. The oxoammonium cation of the polymer, *i.e.* the oxidized state of the polyelectrolyte, was prepared by bulk electrolysis at 1 V *vs.* Ag/AgCl using the H-type cell (EC Frontier Co.) using an ethyl viologen dichloride solution placed in the counter electrode compartment. An anion exchange membrane (SELEMION®, AGC Co., Inc.) was used as the separator during bulk electrolysis.

### Battery test

A prototype flow cell was fabricated using a conventional cell kit obtained from ElectroCell A/S (Micro Flow Cell). Carbon felt (3 cm × 3.3 cm with a thickness of 3 mm, EC Frontier Co.) was employed as the porous electrode. As a separator, a dialysis membrane made of cellulose (MEMBRA-CEL®, Viskase Co. Inc., pore size of 1.25 nm) or anionic exchange membrane (SELEMION®, AGC Co. Inc.) was employed. Liquid delivery pumps obtained from Yamato Scientific Co. Ltd were used for flow circulation. The pumping tube was made of TYGON® resin with an inner diameter of 1/8 inch and an outer diameter of 1/4 inch. The electrolytes (50 mL each) were added to vials and flowed at a rate of 20 mL $min^{-1}$. An airtight H-type cell (EC Frontier Co.) was used for high-capacity (0.75 M, 20 Ah $L^{-1}$) measurements, where the carbon felt porous electrode (0.6 cm × 3.3 cm with 3 mm thickness) and a separator were the same materials as those for the prototype flow cell. The carbon felt was inserted into the platinum wire, which served as the current collector. The electrolyte was stirred to promote mass transfer. All measurements were performed at room temperature near 25 °C. In both cases, excessive amounts of ethylviologen dichloride were used. A vacuum glove box (GBJV065 and GBJPNS3L) manufactured by Glove Box Japan Inc. was used in a nitrogen environment with <1 ppm of oxygen for the preparation of the electrolytes. Battery cycle tests were performed using HJ1020mSD8 or HJ1001SD8 obtained from Meiden Hokuto Corp.

### Permeation analysis

**Quantitative measurement of the permeation ratio in pure water.** A prototype flow cell was fabricated using the conventional cell kit from ElectroCell A/S (Micro Flow Cell). The electrolytic flow cell was assembled in the same way as the battery test. To one vial was added an aqueous solution of the active material (TMA-TEMPO or **P1**). Pure water was added to the counter vial. The two solutions, separated by a membrane separator, were flowed at 20 mL $min^{-1}$ without electrolysis. The active material permeated to the counter vial was collected by using a capillary tube. The amount of the active material permeated through the separator membrane was estimated from the integral ratio of the ESR spectrum. Permeability was defined as 100% when the concentrations in the two vials were equalized so that there was no concentration gradient across the separator membrane. The permeation analysis was performed at room temperature maintained at 25 °C.

**Analysis of permeation behavior under electrochemical conditions.** To evaluate the crossover of the polyelectrolyte during electrolysis, a coupled flow battery setup was constructed using the same flow cell design, membranes, and electrolyte (1 M NaCl aqueous solution) as described above. Two identical cells were connected: one equipped with an anion exchange membrane for electrolysis and the other with a porous dialysis membrane for crossover monitoring. The working compartment of the electrolytic cell was filled with a **P1** solution (1.5 mM, 40 mA h $L^{-1}$), and the counter compartment with ethylviologen dichloride (3.6 mM, 100 mA h $L^{-1}$). These solutions were continuously circulated at 20 mL $min^{-1}$. The same flow rate was maintained in the monitoring cell, where 1 M NaCl was circulated on the opposite side of the nanoporous membrane. Crossover was evaluated by cyclic voltammetry of the solution in the monitoring reservoir using the electrochemical conditions previously described. The presence or absence of a current peak at the oxidation potential of TEMPO ($E \approx 0.76$ V *vs.* Ag/AgCl) was used as the indicator of active species permeation.

## Results and discussion

### Synthesis and characterization of redox-active polyelectrolyte

The TEMPO-substituted polyelectrolyte (**P1**) was designed as a radical polymer with high water-solubility. The design concept was to mitigate the inherent hydrophobicity of the TEMPO moiety by directly substituting an ionic functional group adjacent to the TEMPO moiety. **P1** was synthesized by the free radical polymerization of the ionic monomer followed by oxidation (Scheme 1).

3-(Bromopropyl)acrylamide was synthesized for quaternary ammoniation in the Menshutkin reaction. As an autocyclization reaction has been reported for acrylamide derivatives with a terminally substituted leaving group,[32] the Menshutkin reaction was performed at room temperature to avoid the undesired autocyclization that tends to occur at high temperatures. The slow $S_N2$-type reaction of the bulky tertiary amine with a piperidine moiety took 72 hours to complete. The monomer was obtained in a high yield (>90%). **P1** was synthesized *via* free radical polymerization followed by hydrogen peroxide and sodium tungstate-catalyzed oxidation of the piperidinyl group.[33,34] The molecular weight of **P1** was estimated to be $M_n$ = *ca.* $1.6 \times 10^4$ with a moderate polydispersity of $M_w/M_n = 1.5$. The chemical structures of the monomer and the precursor polymer were identified by $^1$H-NMR (Fig. S1–S5). FT-IR showed typical absorption peaks of IR-active amides (Fig. S6). The nitroxide radical in **P1** was detected by ESR, which revealed a partially broadened three-line hyperfine structure at $g = 2.0067$ for an unpaired electron on the nitrogen atom with a nuclear spin of $I = 2/2$ due to the enhanced spin exchange between the densely populated radicals bound to the polymer backbone. The SQUID magnetization experiment revealed the radical density per monomer structure of **P1** to be 98% (Fig. S7), assuming its paramagnetic properties with $S = 1/2$.

The 5% decomposition temperature of **P1** was estimated to be $T_{d5} = 225$ °C (Fig. S8a). No glass transition temperature ($T_g$) was observed for a temperature range of 50–200 °C, suggesting

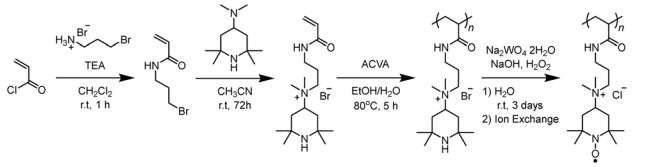


Scheme 1 Synthetic route to the TEMPO-substituted polyelectrolyte (**P1**).

 

its strong coulombic interaction between the ammonium group and the chloride ion (Fig. S8b).

### Solubility and dynamic viscosity of the P1 electrolyte

As shown in Fig. 1 and Table S1, **P1** exhibits the highest charge-storage capacity among water-soluble redox-activepolymers reported to date, while retaining moderate viscosity. While **P1** lost significant flowability at 4 M (107 Ah $L^{-1}$) in 1 M NaCl solution, **P1** is, to our knowledge, the first polymeric redox-active material that is substantially soluble above 4 M. Notably, **P1** dissolved 2 M (54 Ah $L^{-1}$, 241 mPa s), a concentration that far exceeds those of previously reported polymer-based electrolytes. Compared to redox-active electrolytes based on deep eutectic solvents (DES),[35,36] which often exhibit similarity at capacities of 1 M (>26 Ah $L^{-1}$), **P1** demonstrates more than twice the charge-storage capacity without compromising flowability. VRFBs actually operate at only about 25 Wh $L^{-1}$ (20 Ah $L^{-1}$, 1.26 V) due to battery polarization and mass transfer delays. **P1** is the first polymeric active material with the potential to exceed the capacity of VRFBs.

The exceptional solubility and performance of **P1** are attributed to the presence of proximal quaternary ammonium groups, which enhance both hydrophilicity and electrostatic repulsion between chains. These findings indicate that the viscosity threshold, rather than true solubility, is the practical limiting factor at high concentrations. The absence of visible turbidity even at 4 M suggests that the actual solubility limit may lie beyond this point. While further viscosity reduction may be realized by incorporating branched architectures such as hyperbranched or bottle-brush polymers, here we focused on the potential of a linear backbone, demonstrating that high capacity and moderate viscosity are simultaneously achievable.

The effect of the proximal highly hydrophilic ammonium groups in **P1** was pronounced. The upper limit of viscosity was reached prior to solubility, and the actual solubility limit of **P1** was inferred to be above 4 M, based on the apparent transparency of the mixture. While further viscosity reduction should be achieved with branched structures such as hyperbranched[37] and bottle-brush polymers,[38] we focused on the potential of the linear backbone in this study, demonstrating that high concentration and practical flowability can be simultaneously realized.

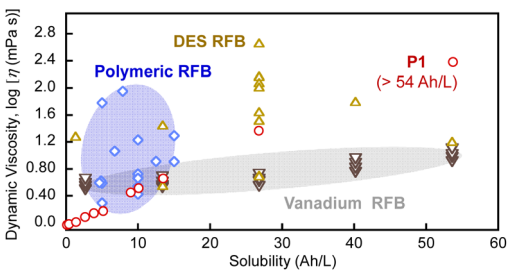


Fig. 1 Mapping of viscosity *versus* charge-storage solubility of various electrolytes for RFBs.

The dependence of viscosity on **P1** concentration was determined to unravel the nature of polyelectrolyte chains in solutions. The estimation of the intrinsic viscosity, $[\eta]$, of polyelectrolytes with salts was based on the proposed equation in a previous report[39] to avoid the nonlinearity associated with increased electrostatic interactions. The oxidized state of **P1**, containing the oxoammonium cation in place of the nitroxide moiety (**P1**$^+$), was prepared by bulk electrolysis. A comparison of the viscosity behaviors of **P1** and **P1**$^+$ revealed an intriguing aspect in that an overall decrease in viscosity was observed for **P1** as it was charged. This trend is in contrast to the previously reported viscosity behavior of ferrocene-substituted copolymers.[18] This distinction is rationalized by the difference in charge density change per monomer unit upon oxidation; conventional redox-active polymers have a maximum charge state of +1 per monomer upon oxidation, whereas the system investigated here shifts from +1 to +2, resulting in greater hydration and structural effects. **P1** achieved high solubility in water due to the proximal ammonium group which counteracted the hydrophobicity of TEMPO. The intrinsic viscosities were determined to be $[\eta] = 4.8$ mL $g^{-1}$ and 3.6 mL $g^{-1}$ for **P1** and **P1**$^+$, respectively (Fig. 2). The viscosity measurements were conducted in a 1 M NaCl aqueous solution in the dilute range of the polymers, so that most of the ammonium groups in the polycation, **P1**, were effectively shielded. As a result, **P1** behaved like a neutral polymer in a hydrated state. The polydication **P1**$^+$ was similarly shielded, but the oxoammonium groups generated a more locally polarized environment than **P1**, attracting hydrated anions beyond the bulk shielding effect. This suggests that the increased local ion density around the oxoammonium groups reduced chain mobility, leading to coil contraction. It should be noted that since the concentration dependence of the viscosity of polymer solutions is discussed in their dilute range, it may differ from the behavior of polymer solutions at higher concentrations actually applied to RFBs. However, the decrease in viscosity upon oxidation of **P1** appears to be advantageous for the discharge of **P1**$^+$ due to the lower energy loss for flowing.

### Electrochemical properties

The redox behavior of TEMPO-substituted polyelectrolytes was evaluated by cyclic voltammetry in an aqueous NaCl solution. A

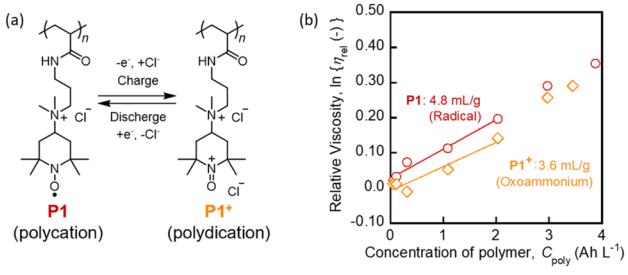


Fig. 2 (a) Redox reaction of the TEMPO moiety in P1 to yield the polydication P1$^+$ bearing the oxoammonium moiety per repeating unit. (b) Concentration dependence of the viscosity of the polyelectrolytes in the charged state P1$^+$ (◇) and the discharged state P1 (○).

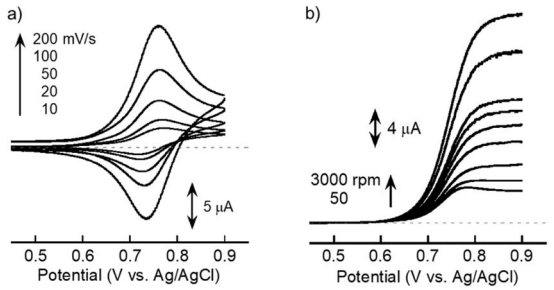


Fig. 3 Voltammetric responses obtained for 2 mM **P1** dissolved in the aqueous electrolyte. (a) Cyclic voltammetry scanned at 10, 20, 50, 100, and 200 mV $s^{-1}$. (b) Hydrodynamic voltammograms. The electrode disk was rotated at 50, 100, 200, 400, 600, 1000, 2000, and 3000 rpm.

reversible redox response was observed for **P1** at $E_{1/2} = 0.74$ V *vs.* Ag/AgCl (Fig. 3a). **P1** exhibited a higher redox potential than conventional TEMPO-substituted polymers.[8,25,26,40–42] The alkylammonium groups that were directly substituted on TEMPO contributed to both hydrophilicity and the redox potential. This is consistent with the high redox potential of monomeric TEMPO derivatives bearing a nitrogen atom substituted at the 4-position.[43]

Diffusional properties of the TEMPO-substituted polyelectrolyte were evaluated by hydrodynamic voltammetry using the same disk electrode (Fig. 3b). Levich plots of the plateau currents *versus* the square root of the electrode rotation rate were linear, suggesting its diffusion-limited behavior at sufficiently high overpotentials (Fig. S9a). The slope of the Levich plots gave the apparent diffusion coefficient $D = 5.6 \times 10^{-7}$ $cm^2$ $s^{-1}$. Koutecký–Levich plots (Fig. S9b) and Tafel plots (Fig. S9c) gave the standard rate constant for the electrochemical reaction $k_0 = 3.9 \times 10^{-3}$ cm $s^{-1}$. The redox-active polyelectrolyte revealed a higher rate constant for the electrode reaction than the previously reported water-soluble copolymers (Table 1), which is similar to the tendency for some low-molecular-weight derivatives.[12,44] The physical diffusion coefficient of the polymer was smaller than that of the corresponding low molecular-weight compounds in agreement with the lower diffusivity of polymers predicted by the Stokes–Einstein equation.

The dense substitution of the TEMPO redox sites in the polymer, which are highly bistable allows for rapid electron transfer,[11] demonstrating the advantages of the redox-active polyelectrolyte-type molecular design. Based on its high-water solubility and electrochemical properties, charging and discharging at a high concentration of 20 Ah $L^{-1}$ (0.75 M) was tested using an airtight H-type cell (Fig. 4). The initial discharge capacity reached 16 Ah $L^{-1}$ with a coulombic efficiency of 95%. The energy efficiency, although above 80%, was relatively low and showed a declining trend over successive cycles. This behavior is attributed to reduced ionic conductivity due to the high viscosity of the electrolyte, resulting in increased overpotential. It also reflects the mixing limitations inherent to static H-type cells. Despite this, the system exhibited stable cycling performance, retaining 94% of its initial discharge capacity, with a moderate average coulombic efficiency (>92%). Nevertheless, this represents the first demonstration of efficient operation at twice the charge-storage capacity of conventional polymeric RFBs, comparable to that of vanadium RFBs.

To investigate capacity fade and low coulombic efficiency, IR spectroscopy was performed on the electrolyte after the cycling test (Fig. S10). During extended operation, a gradual reduction in electrolyte volume was observed, and pH test paper indicated a shift toward acidic conditions. These findings provide strong evidence for parallel oxygen evolution reactions slightly occurring at high potentials, leading to water depletion and acidification. Furthermore, a subtle peak appeared in the IR spectra in the 1750–1700 $cm^{-1}$ region,[45] corresponding to the $^{+}N{=}O$ stretching vibration of the oxoammonium form of oxidized TEMPO. This strongly suggests that the formation of oxoammonium species occurred *via* pH-dependent disproportionation of TEMPO,[46] rather than due to active material degradation or poor utilization.

Overall, the results indicate that capacity fade arises primarily from electrolyte-side reactions and subsequent pH-induced redox transformations, rather than from decomposition of the polymeric active material. Further optimization of supporting electrolyte composition, electrode materials, and pH buffering will be crucial to enhance long-term performance.

## Separator permeation analysis and battery tests using a nanoporous membrane

The large molecular size of **P1**, statistically distributed in the aqueous electrolyte solution with a mean diameter of *ca.* 4 nm (Fig. S11), resulted in significantly reduced permeability

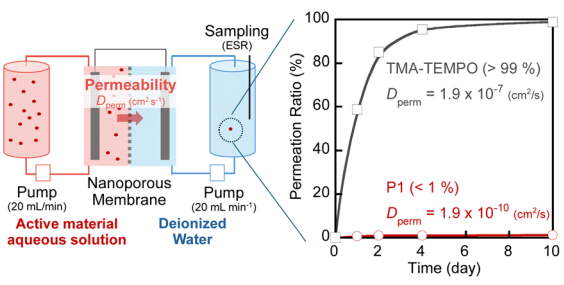


Fig. 4 Configuration of the cell for the permeation test and the related experimental result. The active materials were flowed at 20 mL $min^{-1}$ to proceed with permeation to the other cell with only water.

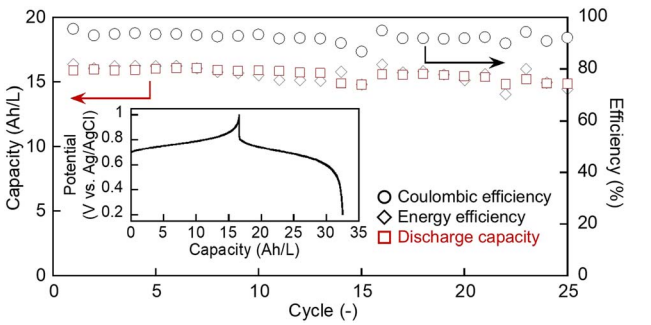


Fig. 5 Cycle performance of the prototype RFB with 0.25 C, 20 Ah $L^{-1}$ (0.75 M). Inset: charge–discharge curves of the 1st cycle.

through the porous membrane separator down to one-thousandth compared to the small molecule TMA-TEMPO (Fig. 5). The reduced permeability for **P1** allowed stable charge–discharge behavior with a high energy efficiency even after 50 cycles using a prototype symmetric cell separated by the porous membrane, which demonstrated the applicability of **P1** for polymer RFBs.

The permeability of small molecules such as TMA-TEMPO and the polyelectrolyte **P1** through the porous membrane was compared under flow conditions regarded as equivalent to those in RFBs (Fig. S12). Deionized water was chosen as the solvent rather than the brine due to its lower permittivity for quantitative detection of the radical from the ESR signal intensity. The permeability exceeded 90% after a few days and was almost saturated when TMA-TEMPO was flowed at 20 mL $min^{-1}$. The permeability of TMA-TEMPO and **P1** was calculated to be $D_{perm} = 1.9 \times 10^{-7}$ $cm^2$ $s^{-1}$ and $1.9 \times 10^{-10}$ $cm^2$ $s^{-1}$, respectively (Fig. S13).

To assess the permeability of **P1** during electrochemical operation, a coupled prototype cell was fabricated (Fig. S14a). One compartment was equipped with an anion exchange membrane for electrolysis, while the other contained a dialysis membrane to monitor crossover. Permeability was evaluated by cyclic voltammetry of the reservoir behind the dialysis membrane ($E = 0.76$ V *vs.* Ag/AgCl), where the appearance of an oxidation peak would indicate crossover of the active species. No current peak was observed at the oxidation potential of TEMPO, suggesting negligible crossover during operation (Fig. S14b). In deionized water, the high chain flexibility of **P1** may allow a small fraction of the polymer to permeate the membrane. By contrast, in 1 M NaCl solution, electrostatic shielding induces chain contraction and reduces flexibility, likely enhancing the polymer's physical exclusion. During continuous operation of the electrochemical compartment under dilute conditions, gradual capacity fade and moderate coulombic efficiency (<90%) were observed (Fig. S14b and c). As no detectable crossover was found in the analysis compartment, these losses are unlikely to result from permeability through the porous membrane. Instead, the observed electrolyte acidification and oxygen evolution (Fig. S14d), similar to those at high concentrations, can reasonably explain the performance decline due to reduced utilization of redox-active species. These findings confirm that **P1** exhibits excellent membrane retention even under electrochemical cycling, and that further improvement in overall efficiency will require optimization of operating conditions and cell components, rather than modification of the active material itself.

## Conclusions

In this study, redox-active polyelectrolytes were proposed as a new strategy of molecular design for active materials in polymeric RFBs. Ionic functional groups were introduced in close proximity to the hydrophobic TEMPO moiety, which dramatically altered its properties to behave as a hydrophilic moiety. The hydrophilic acrylamide main chain, which also contributed to high water-solubility, was synthesized *via* free radical polymerization of the water-soluble monomer obtained by the Menshutkin reaction, which was then subjected to the classical radical generation reaction. The designed polymeric active material achieved high water solubility and a redox potential comparable to or higher than that of previously reported TEMPO-based polymers under similar aqueous NaCl conditions. The polymer retained excellent electrochemical properties based on fast electron transfer and crossover inhibition through the porous separator due to the high density of redox site substitution. Interestingly, dynamic viscosity of the redox-active polyelectrolyte and its intrinsic viscosity decreased with charging, suggesting the enhanced rigidity of the polymer chain due to electrostatic repulsion. The present redox-active polyelectrolyte is the first polymeric active material with the potential to exceed the effective capacity of VRFBs. Analysis of the molecular weight dependence of the intrinsic viscosity should allow characterization of the viscosity properties linked to charging and discharging and especially the viscosity behavior under high concentration conditions, which is the target of our continuous study.

## Author contributions

K. I. conducted the experiments, analyzed the data, and wrote the original draft. K. O. conceived the project, supervised the research, and revised the manuscript. Both authors reviewed and approved the final manuscript.

## Conflicts of interest

There are no conflicts to declare.

## Data availability

The data supporting this article have been included as part of the SI. Supporting Information: Synthetic procedures, NMR spectra, physical and electrochemical properties, and permeation analysis. See DOI: **https://doi.org/10.1039/d5ta03516c**.

## Acknowledgements

This work was supported by the NEDO International Collaborative Study on Next-Generation Grid-Ready Redox Flow Battery Using Nonmetallic Charge Storage Materials (No. 24000741-0). This work was partially supported by the Grants-in-Aid for Scientific Research (No. 21H04695 and 22K18335) from MEXT, Japan. This work was partially supported by Alkali Energy Device Project of Takahata Co. and Waseda University. This work was the result of using research equipment (No. C1027, C1032, C1055, C1056 and C1063) shared in the MEXT Project for promoting public utilization of advanced research infrastructure (Program for supporting construction of core facilities) Grant Number JPMXS0440500025. We thank Assoc. Prof. Takeo Suga for fruitful discussion on redox-active polymer synthesis and properties. We also thank Dr Seigo Watanabe for valuable suggestions.

## Notes and references


1 D. G. Kwabi, Y. Ji and M. J. Aziz, *Chem. Rev.*, 2020, **120**, 6467–6489.
2 S. K. Hazra, H. Kim, H. Meskher, P. Singh, S. Kansara, A. K. Thakur, S. A. Khan, A. M. Saleque, R. Saidur, M. S. Ahmed and J.-Y. Hwang, *Batteries Supercaps*, 2024, **7**, 202400100.
3 Z. Huang, A. Mu, L. Wu, B. Yang, Y. Qian and J. Wang, *ACS Sustainable Chem. Eng.*, 2022, **10**, 7786–7810.
4 C. Minke and T. Turek, *J. Power Sources*, 2018, **376**, 66–81.
5 M. Dassisti, G. Cozzolino, M. Chimienti, A. Rizzuti, P. Mastrorilli and P. L'Abbate, *Int. J. Hydrog. Energy*, 2016, **41**, 16477–16488.
6 P. Leung, A. A. Shah, L. Sanz, C. Flox, J. R. Morante, Q. Xu, M. R. Mohamed, C. Ponce de León and F. C. Walsh, *J. Power Sources*, 2017, **360**, 243–283.
7 Z. Li, T. Jiang, M. Ali, C. Wu and W. Chen, *Energy Storage Mater.*, 2022, **50**, 105–138.
8 K. Hatakeyama-Sato and K. Oyaizu, *Chem. Rev.*, 2023, **123**, 11336–11391.
9 T. Yin, J. Duanmu and L. Liu, *J. Mater. Chem. A*, 2024, **12**, 15519–15540.
10 Y. Y. Lai, X. Li and Y. Zhu, *ACS Appl. Polym. Mater.*, 2020, **2**, 113–128.
11 K. Oyaizu, *Polym. J.*, 2024, **56**, 127–144.
12 T. Janoschka, N. Martin, M. D. Hager and U. S. Schubert, *Angew. Chem., Int. Ed.*, 2016, **55**, 14427–14430.
13 B. Schwenzer, J. Zhang, S. Kim, L. Li, J. Liu and Z. Yang, *ChemSusChem*, 2011, **4**, 1388–1406.
14 J. Ye, L. Xia, H. Li, F. P. G. de Arquer and H. Wang, *Adv. Mater.*, 2024, **36**, 2402090.
15 V. A. Iyer, J. K. Schuh, E. C. Montoto, V. Pavan Nemani, S. Qian, G. Nagarjuna, J. Rodríguez-López, R. H. Ewoldt and K. C. Smith, *J. Power Sources*, 2017, **361**, 334–344.
16 T. Janoschka, N. Martin, U. Martin, C. Friebe, S. Morgenstern, H. Hiller, M. D. Hager and U. S. Schubert, *Nature*, 2015, **527**, 78–81.
17 T. Hagemann, M. Strumpf, E. Schröter, C. Stolze, M. Grube, I. Nischang, M. D. Hager and U. S. Schubert, *Chem. Mater.*, 2019, **31**, 7987–7999.
18 P. S. Borchers, M. Strumpf, C. Friebe, I. Nischang, M. D. Hager, J. Elbert and U. S. Schubert, *Adv. Energy Mater.*, 2020, **10**, 2001825.
19 H. Fu, C. Zhang, H. Wang, B. Du, J. Nie, J. Xu and L. Chen, *J. Power Sources*, 2022, **545**, 231905.
20 K. Hatakeyama-Sato, Y. Igarashi and K. Oyaizu, *RSC Adv.*, 2023, **13**, 547–557.
21 K. Hatakeyama-Sato, K. Sadakuni, K. Kitagawa and K. Oyaizu, *Sci. Rep.*, 2023, **13**, 5711.
22 Y. Igarashi, K. Hatakeyama-Sato, K. Kitagawa, R. Shinozaki and K. Oyaizu, *ACS Appl. Polym. Mater.*, 2024, **6**, 10113–10120.
23 E. Grignon, J. T. Liu, Y. F. Tan, Y. Cao, A. Aspuru-Guzik and D. S. Seferos, *J. Am. Chem. Soc.*, 2025, **147**, 5071–5079.
24 H. Nishide and K. Oyaizu, *Science*, 2008, **319**, 737–738.
25 K. Koshika, N. Sano, K. Oyaizu and H. Nishide, *Macromol. Chem. Phys.*, 2009, **210**, 1989–1995.
26 K. Hatakeyama-Sato, H. Wakamatsu, R. Katagiri, K. Oyaizu and H. Nishide, *Adv. Mater.*, 2018, **30**, 1800900.
27 K. Hatakeyama-Sato, T. Nagano, S. Noguchi, Y. Sugai, J. Du, H. Nishide and K. Oyaizu, *ACS Appl. Polym. Mater.*, 2019, **1**, 188–196.
28 Y. Xie, K. Zhang, Y. Yamauchi, K. Oyaizu and Z. Jia, *Mater. Horiz.*, 2021, **8**, 803–829.
29 B. Hu, M. Hu, J. Luo and T. L. Liu, *Adv. Energy Mater.*, 2022, **12**, 2102577.
30 C. J. Mudugamuwa, Y. Xie, K. Zhang, T. P. Nicholls, J. M. Chalker and Z. Jia, *Green Chem.*, 2023, **25**, 3086–3094.
31 V. Strehmel, H. Rexhausen and P. Strauch, *Tetrahedron Lett.*, 2008, **49**, 3264–3267.
32 D. N. Reddy and E. N. Prabhakaran, *J. Org. Chem.*, 2011, **76**, 680–683.
33 T. N. Pinheiro, E. G. Barbosa and A. K. Jordão, *SynOpen*, 2022, **06**, 208–210.
34 E. Schröter, P. Rohland, K. Schreyer, C. Friebe, M. D. Hager and U. S. Schubert, *Eur. J. Org Chem.*, 2022, **2022**, 202200485.
35 C. Zhang, Z. Niu, Y. Ding, L. Zhang, Y. Zhou, X. Guo, X. Zhang, Y. Zhao and G. Yu, *Chem*, 2018, **4**, 2814–2825.
36 Q. Xu, L. Y. Qin, Y. N. Ji, P. K. Leung, H. N. Su, F. Qiao, W. W. Yang, A. A. Shah and H. M. Li, *Electrochim. Acta*, 2019, **293**, 426–431.
37 K. Ehtiati, I. Anufriev, C. Friebe, I. A. Volodin, C. Stolze, S. Muench, G. Festag, I. Nischang, M. D. Hager and U. S. Schubert, *RSC Adv.*, 2024, **14**, 32893–32910.
38 T. Sukegawa, I. Masuko, K. Oyaizu and H. Nishide, *Macromolecules*, 2014, **47**, 8611–8617.
39 B. A. Wolf, *Macromol. Rapid Commun.*, 2007, **28**, 164–170.
40 K. Koshika, N. Chikushi, N. Sano, K. Oyaizu and H. Nishide, *Green Chem.*, 2010, **12**, 1573.
41 N. Chikushi, H. Yamada, K. Oyaizu and H. Nishide, *Sci. China Chem.*, 2012, **55**, 822–829.
42 K. Sato, R. Katagiri, N. Chikushi, S. Lee, K. Oyaizu, J. S. Lee and H. Nishide, *Chem. Lett.*, 2017, **46**, 693–694.
43 H. Fan, J. Zhang, M. Ravivarma, H. Li, B. Hu, J. Lei, Y. Feng, S. Xiong, C. He, J. Gong, T. Gao and J. Song, *ACS Appl. Mater. Interfaces*, 2020, **12**, 43568–43575.
44 T. Liu, X. Wei, Z. Nie, V. Sprenkle and W. Wang, *Adv. Energy Mater.*, 2016, **6**, 1501449.
45 A. Kumar and B. P. Tripathi, *Electrochim. Acta*, 2024, **480**, 143906.
46 V. Sen and V. Golubev, *J. Phys. Org. Chem.*, 2009, **22**, 138–143.